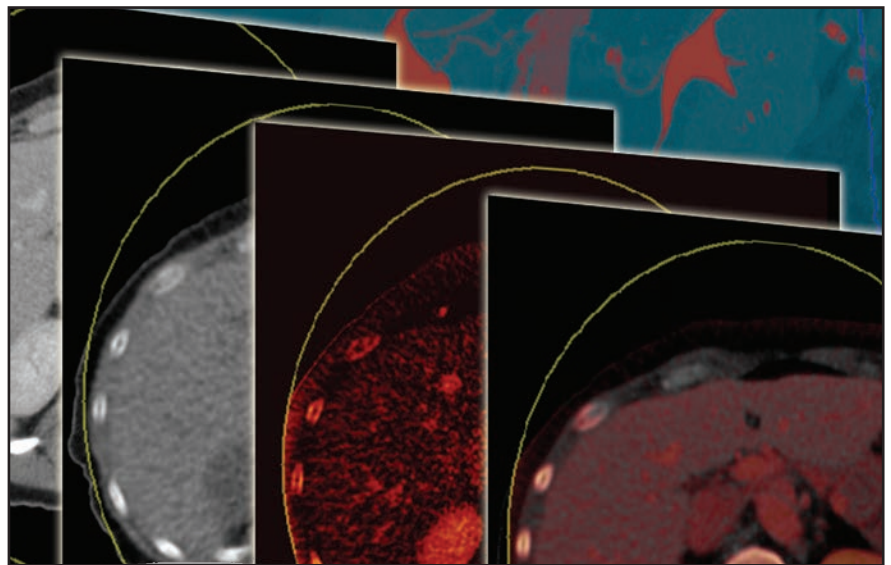


# Abdominal dual-source dual-energy CT: Uses in clinical practice

Marilyn J. Siegel, MD, Juan Carlos Ramirez-Giraldo, PhD, and Anno Graser, MD

**D**ual-energy CT refers to the acquisition of computed tomography (CT) datasets at 2 different energy spectra. The recent development of dual-source scanning has increased the diagnostic value and clinical applications of CT and made dual-energy CT feasible for routine clinical use.<sup>1</sup>

The dual-source system is equipped with 2 x-ray tubes and 2 detector arrays in one gantry, which can be operated at identical tube potentials to produce an increase in temporal resolution in cardiac imaging, photon flux in obese patients or a higher pitch. Additionally, the 2 tubes can be operated independently at different kilovoltage peak (kVp) and milliamperage (mAs) settings. The tube voltages are usually set at 140 kVp for the high-energy tube and at 80 kVp for the low-energy tube. In very obese patients, the low-energy tube can be operated at 100 kVp rather than 80 kVp, which improves the



penetration of low-kVp photons and decreases image noise, making dual-energy CT feasible in larger patients.<sup>1</sup> On the current second-generation scanners, the fields-of-view are 50 cm and 33 cm for the low- and high-energy tubes, respectively. The increased size of the second detector (first generation, 26 cm; second generation, 33 cm) enables coverage of larger anatomical areas.

Second-generation, dual-source, dual-energy CT systems have a selective photon shield made of a tin filter that produces substantial beam hardening, which allows better separation of low- and high-energy spectra (Figure 1). By filtering out low-energy quanta

in the 140-kVp tube, the tin filtering system increases dose efficiency and improves tissue differentiation.<sup>2</sup>

## Image postprocessing

Each dual-energy acquisition from a dual-source CT system automatically generates 3 separate sets of images: 140-kV images, 80-kV images, and a mixed or blended dataset<sup>3,4</sup> (Figure 2). The blended dataset has an overall appearance similar to a traditional 120-kVp single-energy CT image. All 3 images or only one or 2 datasets can be sent to a workstation for review, depending on the radiologist's preference.

Image blending can be linear or non-linear. The linear blending algorithm

*Dr. Siegel is at the Mallinckrodt Institute of Radiology, Washington University School of Medicine, St. Louis, MO, and Siemens Healthcare, Malvern, PA; Dr. Ramirez-Giraldo is at Siemens Healthcare, Malvern, PA; and Dr. Graser is at University of Munich, Munich, Germany.*

*Disclosure: Dr. Siegel is a speaker for Siemens Healthcare and receives honoraria; Juan Carlos Ramirez-Giraldo is an employee of Siemens; and Dr. Graser is a speaker for Siemens Healthcare.*

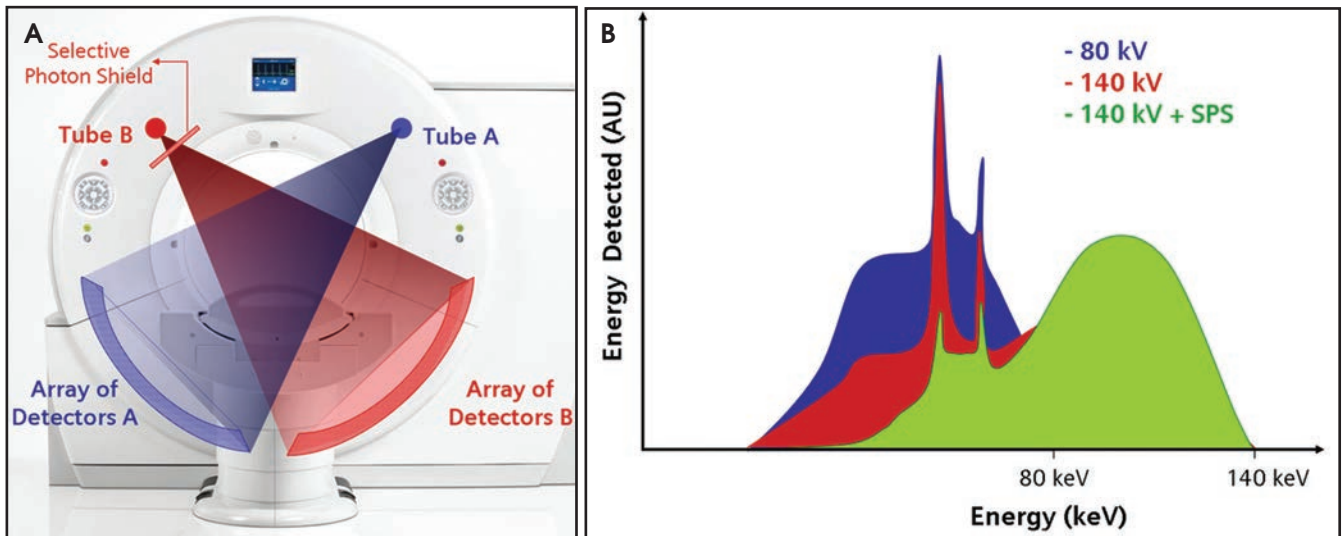


**FIGURE 1.** Dual-source CT system. (A) This scanner has 2 x-ray tubes separated by approximately 90 degrees with corresponding detector arrays. The second-generation system includes a selective photon shield, made of a flat tin filter, which is added to the high-kilovoltage (140 kVp) tube. (B) Comparison of x-ray energy spectra in dual-energy CT. The addition of the selective photon shield (SPS) increases spectra separation relative to 80-kVp spectrum. The increased spectra separation improves dual-energy postprocessing and enables radiation-dose neutrality, relative to conventional single-energy CT.

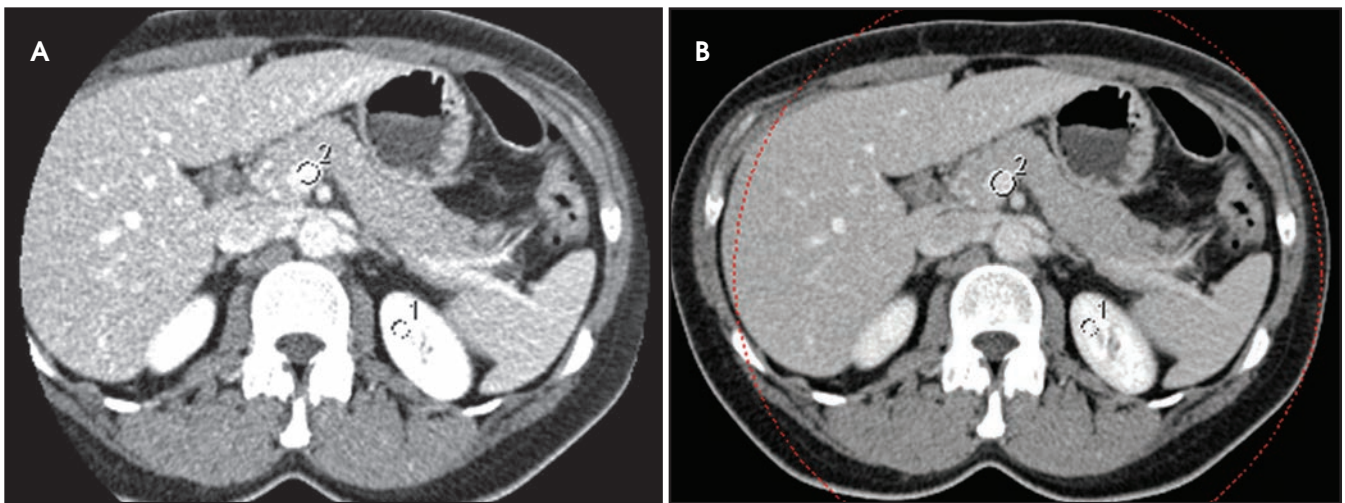


**FIGURE 2.** These are kVp images generated from a dual-energy scan in the late arterial phase. (A) 80-kVp transverse CT image at the level of the pancreas. A small hypervascular-neuroendocrine tumor (2) is noted in the pancreatic head with a mean density of 248 HU, while the renal parenchyma (1) shows a density of 321 HU. Note also the high density of the abdominal aorta. 80-kVp images optimize the attenuation of iodine compared to lower kVp images (see part B below). (B) Weighted average transverse CT image from the same scan using 70% of data from the high and 30% from the low-kVp scan. The hypervascular tumor (2) now measures 160 HU, and the renal parenchyma (1) shows a density of 203 HU. The dotted circle represents the field-of-view in which dual-energy processing is applied. In larger patients, the lateral aspect of the abdomen may not be included in the dual-energy field-of-view.

uses a specific percentage of the low- and high-energy scans.<sup>4</sup> In general, 80-kVp images have more contrast and more image noise, whereas 140-kVp images have less noise and less inherent contrast. The usual default-weighting ratio is 0.5 (50% contribution from each of the high and low energies). However, depending on the desired amount of contrast or noise, blending ratios can

range from 0.3 to 0.7. For instance, with a ratio of 0.7, 70% of the contribution is from 80-kVp images and 30% from 140-kVp images.

Nonlinear blending is based on modified sigmoid blending and operates in a voxel-by-voxel fashion.<sup>3</sup> Blending can increase the contrast-to-noise ratio by accentuating the brightest voxels (containing iodine) from the low-kVp

images and by using the lower noise characteristics of voxels in the high-energy kVp image (Figure 3). In addition, virtual unenhanced CT images, iodine maps, color-coded images superimposing iodine distribution on the virtual nonenhanced data, bone-subtraction images for CT angiographic studies, and renal stone content analytic images can be generated using dual-energy

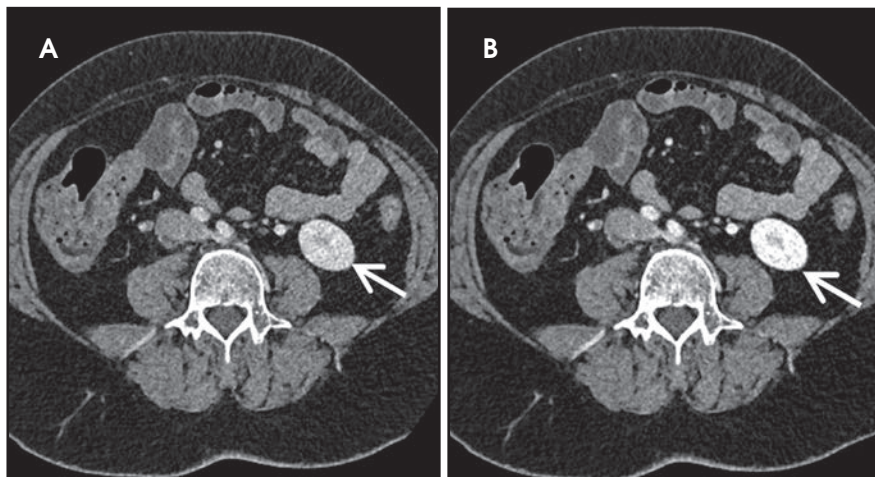


**FIGURE 3.** Linear vs. nonlinear blending. (A) Mixed image using linear blending of 30% of the low-kVp image and 70% high-kVp image. Note relatively low-contrast signal in the left kidney (arrow). (B) Mixed image using nonlinear blending algorithm. Nonlinear blending increases the contrast-to-noise ratio by accentuating the iodine-containing voxels from the low-kVp images. Note the higher attenuation of the renal parenchyma (arrow).

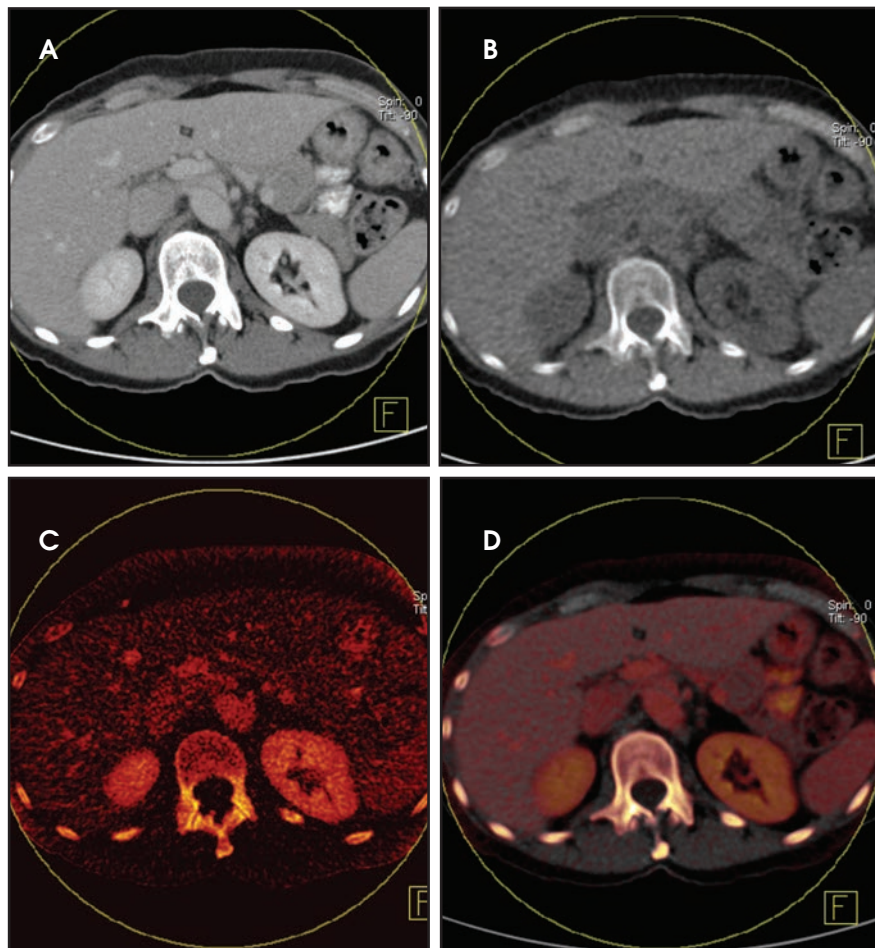


**FIGURE 4.** Postprocessed images generated from a dual-energy portal-venous phase CT examination of the abdomen. (A) Weighted-average image that simulates a standard 120-kVp CT image. (B) Virtual nonenhanced image. (C) Iodine map, which accentuates flow in vascular structures. (D) Superimposition of the iodine map onto virtual nonenhanced image, which improves anatomic definition.

postprocessing software (Figures 4 and 5).

**Limitations**

One potential limitation of dual-energy CT is that the second detector has a small field-of-view. This means that in large patients, the periphery of the patient may not be included in the field-of-view, which limits the ability to use color-coded or virtual unenhanced images in the peripheral regions of the scanned volume. This field-of-view limitation is not a problem for evaluation of the aorta, adrenal glands, pancreas, or small bowel, but it may limit evaluation of some renal masses. Secondly, datasets acquired at 80 kVp or 100 kVp inherently have more noise than images acquired at 120 kVp or 140 kVp, and image noise will substantially increase in large patients.

**Applications in the abdomen**

**Kidney**

**Renal tumors**—Dual-energy CT can improve the characterization of small indeterminate renal lesions found incidentally on contrast-enhanced images. In this setting, the common differential diagnostic considerations are hyperattenuating cysts and a renal mass. The CT differentiation of benign and malignant masses is based on demonstrating the presence of lesion enhancement and the attenuation value of the lesion. Because the K-edge of iodine (33.2 keV) is closer to lower energies (80 kVp) than it is at higher energies (140 kVp), the attenuation of iodine is higher at lower energies. Thus, renal cancers will have higher attenuation than hyperdense cysts at 80-kVp datasets, related to the differences in the amount of iodine within these different lesions. Color-coded images that show the distribution of iodine within the scanned tissue volume are also helpful to show intratumoral enhancement (Figure 6).

Using a virtual unenhanced dual-energy image, baseline attenuation measurements can be made, thereby obviating true unenhanced imaging and reducing the radiation exposure.<sup>1,5,6</sup>



**FIGURE 5.** Bone subtraction from dual-energy CT angiography. Coronal multi-planar reformation after bone subtraction shows occlusion of the left distal external iliac artery (arrow).

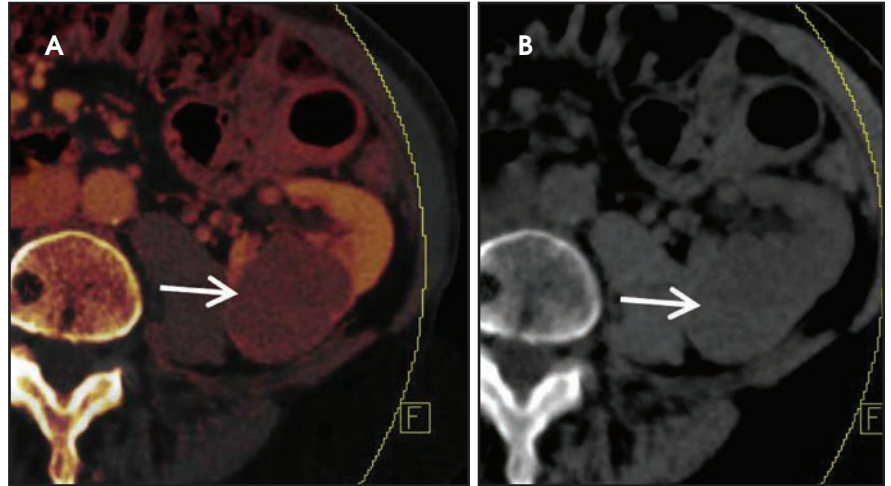


**FIGURE 6.** Dual-energy CT in the characterization of renal masses. (A) The iodine map shows a well-defined mass in the left kidney. The lesion shows iodine uptake (orange color) (arrow), indicating a vascular mass. (B) On the virtual nonenhanced image, the mass (arrow) is iso-attenuating to renal parenchyma, indicating a solid tumor, rather than a cystic mass. Histopathology showed papillary renal-cell carcinoma.

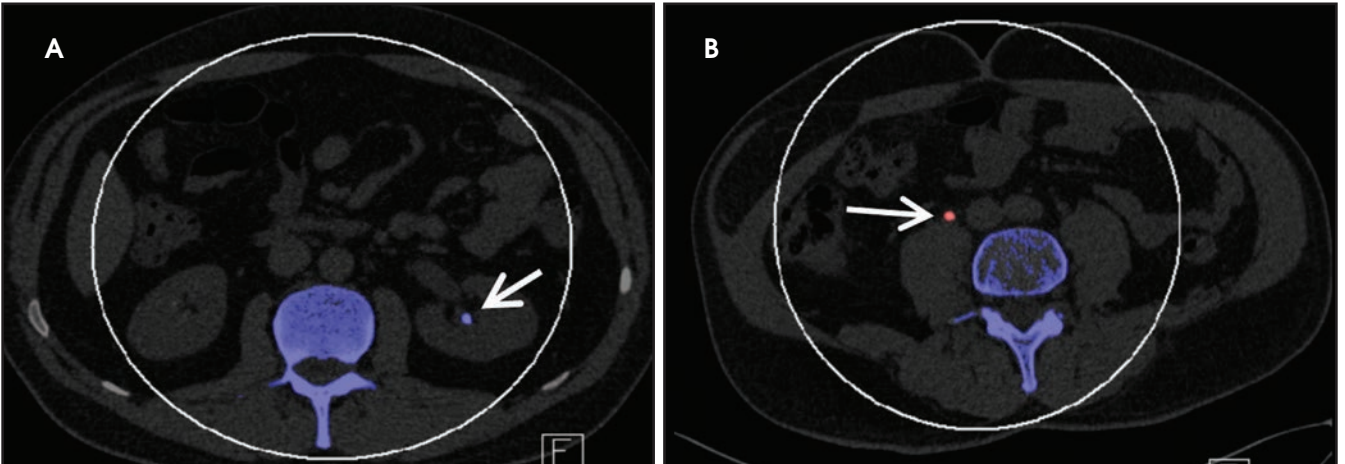


**FIGURE 7.** Dual-energy CT in renal stone characterization. (A) Calcium oxalate stone in the left renal pelvis (arrow) is coded blue. Note the density of the renal calculus is similar to that of bone. (B) Uric-acid stone in the mid-right ureter (arrow) is coded red.

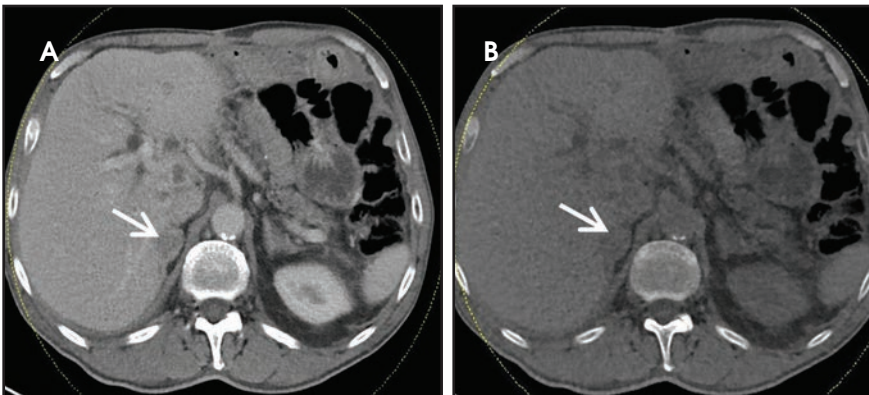


**FIGURE 8.** Right adrenal nodule incidentally found in a patient with cholangiocellular carcinoma. (A) On the venous phase weighted average image, the adrenal nodule (arrow) has an attenuation value of 35 HU. (B) On the virtual nonenhanced image generated from the same dataset, the nodule (arrow) has an attenuation of 7 HU, a value that is diagnostic for an adenoma.

Preliminary data support good correlation between Hounsfield units (HU) in the renal parenchyma on virtual unenhanced and true unenhanced images. Graser et al reported mean density values of  $30.8 \pm 4.0$  HU (true unenhanced CT) and  $31.6 \pm 7.1$  HU (virtual unenhanced CT) ( $p=0.26$ ).<sup>9,10</sup> Using virtual unenhanced datasets, these authors also reported that tumors have a higher density (mean  $105.7 \text{ HU} \pm 73.6$ ) than complicated renal cysts (mean,  $55.0 \text{ HU} \pm 15.8$ ), allowing them to be reliably identified and characterized. By comparison, simple renal cysts have attenuation similar to water ( $2.1 \text{ HU} \pm 1.3$ ).<sup>6</sup>

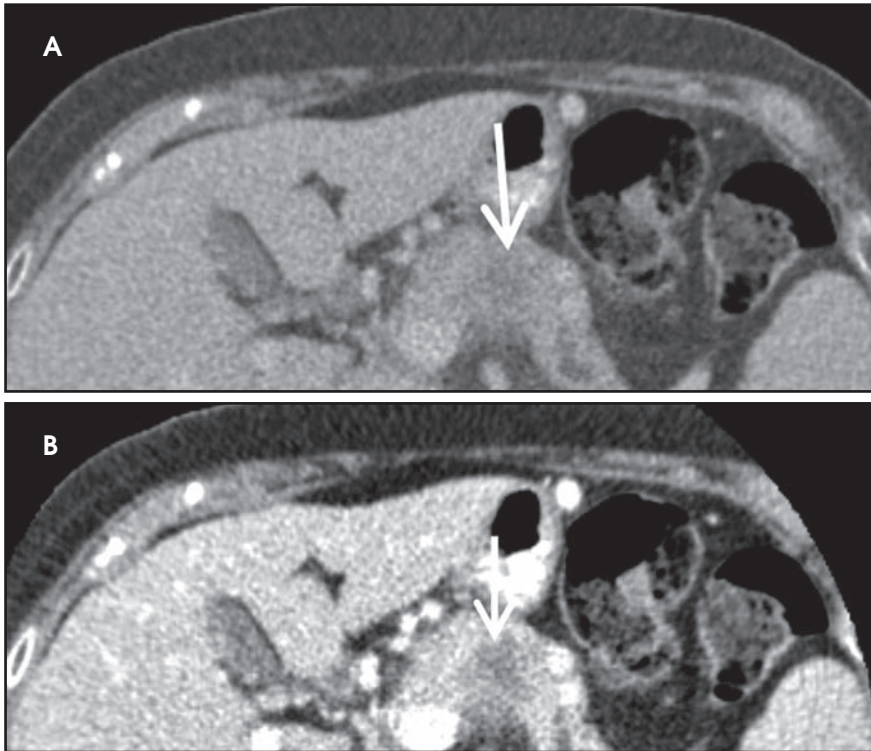


**FIGURE 9.** Dual-energy CT in a patient with adenocarcinoma of the pancreatic body (arrow). (A) On the 120-kVp image, the pancreatic mass (arrow) is poorly defined. (B) On the 80-kVp image, the lesion (arrow) is more conspicuous due to a larger difference in attenuation between the tumor and the surrounding pancreatic parenchyma. Note also increased attenuation/conspicuity of the hepatic vessels.

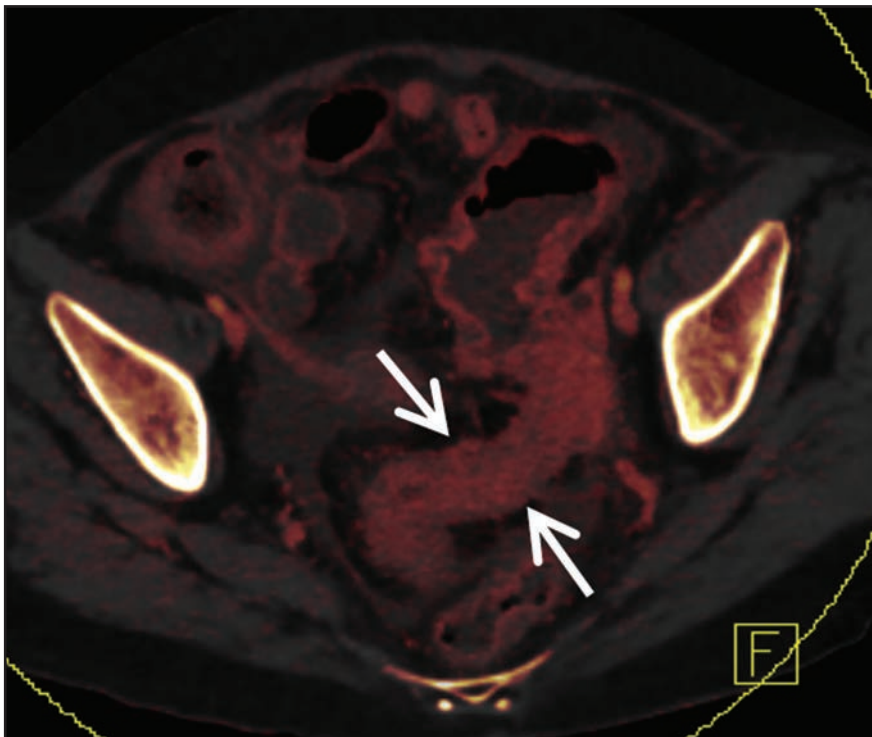


**FIGURE 10.** Dual-energy color-coded iodine overlay image in a patient with ulcerative colitis shows increased enhancement of the wall of the sigmoid colon (arrows) indicating active inflammatory bowel disease.

**Urinary calculi**—In patients with flank pain and suspected urinary calculi, unenhanced single-energy CT is the imaging test of choice for reliable detection and localization of calculi. However, it cannot determine the chemical composition of renal calculi. The 3 frequent types of renal stones are calcified stones (calcium oxalate), uric-acid and struvite stones (ammonium, magnesium, and phosphate). Characterization of stone composition is of clinical importance because it influences treatment options. Uric-acid stones usually are treated medically by urine alkalization, while calcium and struvite stones may need to be removed mechanically or crushed by extracorporeal shock-wave lithotripsy.

Both in vitro and clinical dual-energy CT studies have shown the feasibility of differentiating uric-acid stones from calcified renal calculi based on material decomposition methods.<sup>7,8</sup> Dual-energy CT postprocessing software algorithms analyze the dual-energy behavior of the calculi and color code them in red when uric acid is detected, and in blue when calcified stones are detected (Figure 7). Voxels with other dual-energy behaviors remain grey. In addition, research studies have shown differentiation of struvite and cysteine stones is possible by adapting the slope of the three-material decomposition algorithm.<sup>7</sup>

**Liver**

Incidental sub-centimeter, hypoattenuating lesions, considered too small for characterization, are often seen in the liver at CT. Although such lesions generally are presumed to be benign in many patients, in oncologic patients, the concern for malignancy increases. Dual-energy CT of the liver can enable detection and differentiation of cysts and hemangiomas from solid tumors.

Scanning at 80 kVp, which increases the attenuation of iodine, and generation of iodine color-coded images that show the iodine distribution in the lesion, can help increase sensitivity for detection of subtle intralésional contrast enhancement, thereby

improving differentiation of hypervascular malignancies from cysts.

The dual-energy data can also be used to generate virtual unenhanced images, which can be used for density measurement, thereby obviating true unenhanced imaging and minimizing radiation exposure.<sup>9,10</sup> In a study of 93 patients, Zhang et al<sup>10</sup> showed that focal hepatic lesions had similar CT-density measurements and contrast-to-noise ratios on virtual unenhanced and true unenhanced images.

### Adrenal gland

An incidental adrenal mass is not an infrequent finding on contrast-enhanced abdominal CT examinations. The main differential diagnostic considerations are adenoma, metastasis, and solid masses, such as adrenal carcinoma and pheochromocytoma.

Dual-energy CT with generation of virtual unenhanced datasets can be used for the differentiation of lipid-rich adenomas from solid adrenal masses.<sup>11,12</sup> Adrenal adenomas will show low mean-attenuation values (< 10 HU on unenhanced images), compared with other masses, such as metastases or pheochromocytomas (Figure 8).

### Pancreas

The normal pancreas enhances substantially during the pancreatic phase and contains more iodine than a pancreatic adenocarcinoma. At 80-kVp imaging, the attenuation of iodine will be greater than that at 140-kVp images, improving differentiation of abnormal and normal tissues, thereby increasing the conspicuity of hypoattenuating pancreatic masses (Figure 9). In addition, color-coded images, by showing reduced iodine uptake, can increase sensitivity for detection of hypovascular pancreatic masses.

### Bowel

The diagnostic criteria of bowel disease include wall thickening and increased enhancement of the bowel

wall. On conventional single-energy CT images acquired at 120 kVp, it can be difficult to differentiate between physiological and abnormal enhancement of the small-bowel wall. Since the attenuation of an iodinated contrast agent increases at low-kVp images, dual-energy CT datasets viewed at 80 kVp can help to increase conspicuity of hypervascular bowel-wall related to inflammatory bowel disease. Color-coded images are also useful for showing subtle contrast enhancement (Figure 10). Similarly, in the setting of small-bowel ischemia, the differences in enhancement between poorly perfused ischemic small-bowel and adjacent well-perfused segments may be accentuated on 80-kVp and color-coded images.

### Radiation exposure

Dual-source, dual-energy CT can provide excellent image quality without an increase in radiation dose compared with single-energy CT. Based on current literature, the effective doses in the abdomen are 3 to 12 mSv.<sup>1,5</sup> Dual-energy CT decreases radiation dose by 1) the addition of tin filtration and 2) elimination of noncontrast images. The tin filtration system increases dose efficiency by eliminating spectral overlap. By generating virtual nonenhanced images, dual-energy scanning obviates true noncontrast scanning with consequent dose reduction.

### Conclusion

With the advances in CT technology capable of dual-energy CT, an increasing number of clinical applications have been reported. Generation of virtual unenhanced images can eliminate acquisition of true unenhanced acquisitions. Thus, a single contrast-enhanced acquisition can yield both unenhanced and contrast-enhanced CT data, which may increase diagnostic accuracy in evaluating the abdominal organs and viscera and can be used to decrease radiation exposure. The attenuation of vessels is substantially higher

at 80-kVp imaging than at 140-kVp imaging, which can improve tumor detection and evaluation of vessels and bowel disease. Radiation doses are comparable with conventional single-energy CT studies.

### REFERENCES

1. Megibow AJ, Sahani D. Best practice: Implementation and use of abdominal dual-energy CT in routine patient care. *AJR Am J Roentgeol.* 2012;199:S71-S77.
2. Primak AN, Ramirez-Giraldo JC, Eusemann CD, et al. Dual-source dual-energy CT with additional tin filtration: Dose and image quality evaluation in phantoms and in vivo. *AJR Am J Roentgeol.* 2010;195:1164-1174.
3. Holmes DR, Fletcher JG, Apel A, et al. Evaluation of non-linear blending in dual-energy computed tomography. *Eur J Radiol.* 2008; 68:409-413.
4. Yu L, Primack AN, Liu X, McCollough CH, et al. Image quality optimization and evaluation of linearly mixed images in dual-source dual-energy CT. *Med Phys.* 2009;36:1019-1024.
5. Graser A, Johnson TR, Chandarana H, Macari M. Dual energy CT: Preliminary observations and potential applications in the abdomen. *Eur Radiol.* 2009;19:13-23.
6. Graser A, Johnson TR, Hecht EM, et al. Dual-energy CT in patients suspected of having renal masses: Can virtually nonenhanced images replace true nonenhanced images? *Radiology.* 2009;252:433-440.
7. Graser A, Johnson TR, Bader M, et al. Dual-energy CT characterization of urinary calculi: Initial in vitro and clinical experience. *Invest Radiol.* 2008;43:112-119.
8. Thomas C, Heuschmid M, Schilling D, et al. Urinary calculi composed of uric acid, cystine, and mineral salts: Differentiation with dual-energy CT at a radiation dose comparable to that of intravenous pyelography. *Radiology.* 2010;57:402-409.
9. Mahgerefteh S, Blachar A, Fraifeld S, Sosna J. Dual-energy derived virtual nonenhanced computed tomography imaging: Current status and applications. *Semin Ultrasound CT MR.* 2010;31:321-327.
10. Zhang LJ, Peng J, Wu SY, et al. Liver virtual non-enhanced CT with dual-source, dual-energy CT: A preliminary study. *Eur Radiol.* 2010;20:2257-2264.
11. Gnannt R, Fischer M, Goetti R, et al. Dual-energy CT for characterization of the incidental adrenal mass: preliminary observations. *AJR Am J Roentgeol.* 2012;198:138-144.
12. Ho LM, Marin D, Neville AM, et al. Characterization of adrenal nodules with dual-energy CT: can virtual unenhanced attenuation values replace true unenhanced attenuation values? *AJR Am J Roentgeol.* 2012;198:840-845.

### Products used

- Somatom Definition Flash, Siemens Healthcare, Forchheim, Germany